Grid simulator for power quality assessment of micro-grids

Carrasco, Joaquin Eloy Garcia; Vasquez, Juan Carlos; Guerrero, Josep M.

Published in:
IET Power Electronics

DOI (link to publication from Publisher):
10.1049/iet-pel.2012.0541

Publication date:
2013

Document Version
Early version, also known as pre-print

This document is a preprint of the paper:
Joaquin Eloy-García, Juan Carlos Vasquez, Josep M. Guerrero "Grid simulator for power quality assessment of micro-grids". Published in IET Power Electronics. doi: 10.1049/iet-pel.2012.0541
ISSN 1755-4535

Grid Simulator for Power Quality Assessment of Micro-Grids

Joaquín Eloy-García[a], Juan C. Vasquez[b] and Josep Guerrero[b]

[a] Department of Electrical Engineering, Carlos III University of Madrid,

C/ Butarque 15, 28911, Leganés, Madrid, Spain

e-mail: jeloygar@ing.uc3m.es

[b] Department of Energy Technology, Aalborg University,

Pontoppidanstraede 101, 9200, Aalborg, Denmark

e-mail: juq@et.aau.dk, joz@et.aau.dk

Abstract

In this paper, a grid simulator based on a back-to-back inverter topology with resonant controllers is presented. The simulator is able to generate three-phase voltages for a range of amplitudes and frequencies with different types of perturbations, such as voltage sags, steady state unbalanced voltages, low order harmonics and flicker. The aim of this equipment is to test the performance of a given system under such distorted voltages. A prototype of the simulator, consisting of two inverters connected back-to-back to a 380 V three-phase grid and feeding a micro-grid composed of two inverter interfaced distributed generators and a critical load was built and tested. A set of experimental results for linear purely resistive loads, non-linear loads and current controlled inverters is presented to prove the capabilities of the simulator. Finally, a case study is presented by testing a micro-grid.

Index Terms

Grid Simulator, Power Quality, harmonics, unbalance, voltage sag, micro-grid, self-healing.

I. Introduction

In recent years, micro-grids (MGs) have attracted a lot of attention from researchers in multiple disciplines, as they could be a starting point for future Smart Grids [1], [2]. Topics like energy management [3], [4], policies and regulations [5], economics [6], stability [7], protections [8], communications [9] and so on, are being investigated. Like many other power electronics-based systems, MGs are likely to be subjected to power quality (PQ) issues like Low Voltage Ride Through (LVRT), imbalances, harmonic compensation and flicker among others [10], [11], [12]. The origin for such voltage disturbances in real distribution systems is usually quite heterogeneous and hardly predictable.

In this scenario, a grid simulator capable of generating such distorted voltages in a fully controlled way becomes an essential tool to test MG performance regarding power quality [13], [14], [15], [16]. A voltage sag, swell and flicker generator is presented in [13], based on an H-bridge inverter and a series transformer for high voltage custom

power devices, thus being a different topology and application than the one presented here. In addition, unbalanced and harmonic voltages are not generated. A similar topology to the one presented here was proposed in [14]. In that case, line side converter had a simple L filter and the DC link capacitor was bulky, which reduces DC link voltage transients, and the state-space control with pole placement was used. The results were presented for a resistive load only. In [15], a single-phase grid simulator based on an H-bridge was used with PI controllers in a $d-q$ reference frame. Only voltage amplitude and frequency variations were tested. Two back-to-back connected inverters are used as a micro-grid interface in [16], providing the frequency and power quality isolation between the utility and the micro-grid. In this case, the back-to-back inverters are used to facilitate the control of the power flow between the utility and the micro-grid and to protect the micro-grid in case of faults, by disconnection from the utility and the consequent transition to islanded mode of operation. For the micro-grid, a topology with two distributed generators and a load at the point of common coupling is used, like in the case study presented here. Load sharing and transition between grid-connected and islanded modes are investigated throughout the paper, but no power quality tests were made. Only simulation results are presented. The same authors proposed a power quality enhanced operation mode in [17], by virtue of compensating the local load current, thus eliminating the non-linearity and unbalance from the voltage at the point of common coupling. Simulation results are presented to show the performance. Similarly, reduction of voltage harmonics is presented in [18], whereas negative sequence compensation for a stiff micro-grid is proposed in [19]. In [18], a selective harmonic elimination technique is proposed, but no information is provided about the source of the voltage harmonics. In the case of [19], a slip ring induction generator is feeding a load through a transformer and the unbalance is obtained with a phase-to-neutral connection of a single-phase load at the secondary of the transformer. In both cases, the focus is to propose a control algorithm to improve a certain power quality aspect of the micro-grid.

By using the proposed grid simulator, these kinds of PQ tests can be performed in a fully controlled way at any voltages and frequencies within the required range, thus increasing the repeatability and effectiveness of the tests. Moreover, the voltage disturbances can be set to meet different requirements depending on the standards and grid codes to be fulfilled. The previous experience in wind or photovoltaic energy integration, with the adaptation of their grid codes in many countries, like Spain [20], Germany [21], Italy [22] and USA [23] and coming countries like the United Kingdom [24], France [25] or China [26], makes it likely to occur in micro-grids as well, specially considering the MG as a whole, which is composed by a number of inverter interfaced generators and loads, such as wind farms, PV plants, energy storage systems, back-up energy systems and electronic loads. There are some requirements in [27], applicable to distributed resource island systems and covering some of the mentioned PQ aspects. So far, however, there are no specific grid codes dealing with this matter for micro-grids.

In this paper, a whole set of tests with linear and non-linear loads and inverters as distributed generators is shown to validate the proposed resonant controller approach. In addition to these general tests, a case study of unbalanced voltage compensation in a micro-grid is also presented in section V.

The paper was divided into six parts. The first part is this brief introduction to the problem. After that, in section II, both grid side and MG side inverter controllers are briefly explained, with more emphasis on the micro-grid side

inverter control, which is the inverter generating distorted voltages to the micro-grid. Section III gives a description of the hardware used for the grid simulator prototype and its main characteristics. The results of the experimental tests are shown in section IV, while section V includes the above mentioned case study for cooperative unbalanced voltage compensation in a micro-grid. Finally, the main conclusions are presented in section VI.

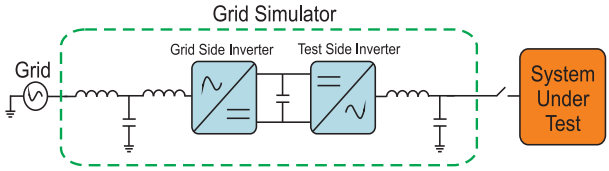

Fig. 1. One-line circuit of the grid simulator prototype with the system under test.

II. Grid simulator control

The proposed grid simulator and the tested system are shown in Fig. 1. It consists of a back-to-back connection of two inverters with LCL and LC filters. The parameters of the inverters are presented in Table I. It was used to generate distorted voltages to both passive loads and inverter loads, as a way of testing the performance of grid-connected systems and components during such perturbations. The inverter loads represent different distributed generators in the tested system, such as a small PV plant and a wind farm in a micro-grid. In addition, also linear and non-linear loads were tested. In this section, a brief description of the controllers of the inverters is presented.

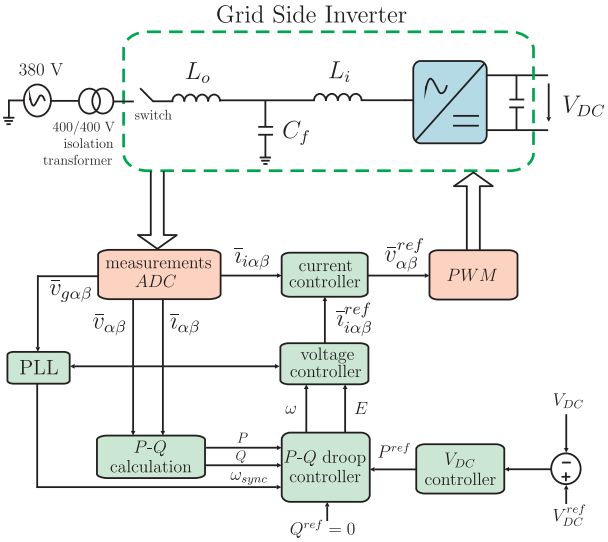

Fig. 2. Control diagram of the grid side inverter.

A. Grid side inverter control

The control diagram of the grid side inverter is shown in Fig. 2, where, together with all physical components (inverter, LCL filter, switch and grid transformer), all control loops have been depicted: 1) current and AC voltage inner control loops; 2) power control loops; 3) DC voltage control loop.

Description	Symbol	Value
Inverter inductor	L_i	1.8 mH
Output inductor	L_o	1.8 mH
Filter capacitor	C_f	27 μF
DC link capacitor	C_{dc}	1100 μF
Switching frequency	f_{sw}	10 kHz

TABLE I
PARAMETERS OF THE INVERTERS.

1) Inner control loops: Ideal proportional-resonant (P-Res) controllers were used for currents and AC voltages, as the use of damping factors is not recommended, since there is no benefit to be gained, as they reduce the gain of the resonant term but do not reduce the sensitivity of the system to variations in the fundamental frequency [28], [29]. The equations of the resonant voltage and current controllers are

$$G_v(s) = K_{pv}\frac{s^2 + \frac{K_{iv}}{K_{pv}}s + \omega^2}{s^2 + \omega^2} \tag{1}$$

$$G_i(s) = K_{pi}\frac{s^2 + \frac{K_{ii}}{K_{pi}}s + \omega^2}{s^2 + \omega^2}, \tag{2}$$

where K_{pv}, K_{iv}, K_{pi} and K_{ii} are proportional and integral gains for voltage and current controllers respectively, and ω is the resonant frequency. For harmonics, pure resonant controllers were used and, similarly, K_{ivh} and K_{iih} are the gains for the h^{th} voltage and current harmonics

$$G_{vh}(s) = K_{ivh}\frac{s}{s^2 + (h\omega)^2} \tag{3}$$

$$G_{ih}(s) = K_{iih}\frac{s}{s^2 + (h\omega)^2}. \tag{4}$$

2) Power control loops: The controllers for active and reactive powers are based on the power flow principle, by regulating w and E

$$\omega = \omega^* + \omega_{sync} + \left(K_{pP} + \frac{K_{iP}}{s}\right)(P - P^*) \tag{5}$$

$$E = E^* + \left(K_{pQ} + \frac{K_{iQ}}{s}\right)(Q - Q^*), \tag{6}$$

where ω^* is the reference frequency, i.e. the fundamental frequency of the grid, ω_{sync} is the synchronization frequency from the PLL, E^* is the amplitude of the voltage reference, i.e. the grid voltage amplitude, and K_{pP}, K_{iP}, K_{pQ} and K_{iQ} are proportional and integral gains for active and reactive power PI controllers respectively. Their values are shown in Table II. The reference for active power P^{ref} is obtained from the DC link voltage controller, as is shown in the next section.

Description		Symbol	Value
Voltage controller	proportional	K_{pv}	2
	fundamental	K_{iv}	8.88
	5^{th} harmonic	K_{iv5}	50
	7^{th} harmonic	K_{iv7}	100
	11^{th} harmonic	K_{iv11}	50
Current controller	proportional	K_{pi}	2.1
	fundamental	K_{ii}	500
	5^{th} harmonic	K_{ii5}	500
	7^{th} harmonic	K_{ii7}	1000
Power controllers	P - proportional	K_{pP}	0.0005
	P - integral	K_{iP}	0.0015
	Q - proportional	K_{pQ}	0.01
	Q - integral	K_{iQ}	0.05
DC link controller	proportional	K_{pdc}	10
	integral	K_{idc}	40

TABLE II
PARAMETERS OF THE CONTROLLERS FO THE GRID SIDE INVERTER.

3) DC link control loop: As well as for power controllers, the DC link voltage is controlled by a Proportional-Integral controller (PI). Its output, as a balance of the energy in the capacitor, is the reference for active power P^{ref}, as shown in Fig. 2. In this case, the dynamic response of this controller must be slower than that of the active power controller for stability reasons, but at the same time, fast enough to deal with the power coming from the test side inverter. The values for the gains of this controller are also shown in Table II.

B. Test side inverter control

The control structure for the test side inverter is basically the same as the previous one, but without the power control loop and the DC link voltage control. The controller parameters are given in Table III. Thus, only the voltage reference generation block, Fig. 3, is explained in this section. The voltage reference for the grid simulator is obtained by the addition of three components:

1) Voltage sag generator: This block is able to generate balanced and unbalanced voltage sags for a given set of inputs, such as sag depth, sag duration and type. For unbalanced sags, setting the sag duration to infinite causes a permanent imbalance in voltage.

In the case of a three-phase sag, all voltages are simultaneously reduced to a value $p|V^{ref}|$, p times smaller, where p is defined as the per unit remaining voltage during the sag, directly related to the sag depth. In this case, the angles between the three phases do not change. Nevertheless, when an unbalanced voltage sag takes place, not only the voltage amplitude but also the phase angles are affected, as is the case of a phase-to-phase voltage sag between phases A and B, shown in Fig. 4. This corresponds to a voltage sag type C [30]. In this case, phase-to-neutral voltage V_c remains

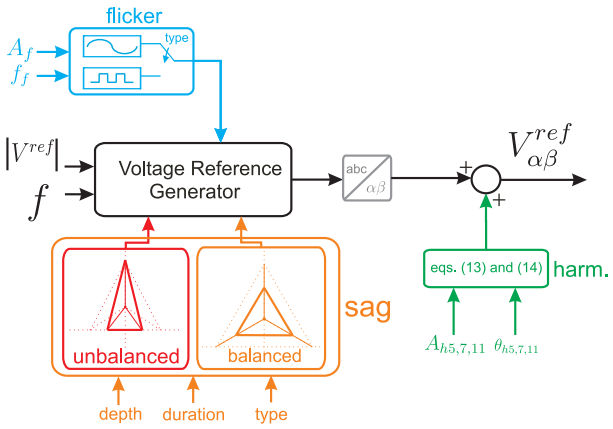

Fig. 3. Scheme of the voltage reference generator.

Description		Symbol	Value
Voltage controller	proportional	K_{pv}	0.5
	resonant	K_{iv}	200
	5^{th} harmonic	K_{iv5}	30
	7^{th} harmonic	K_{iv7}	8
	11^{th} harmonic	K_{iv11}	200
Current controller	proportional	K_{pi}	1
	resonant	K_{ii}	50
	5^{th} harmonic	K_{ii5}	30
	7^{th} harmonic	K_{ii7}	30

TABLE III
PARAMETERS OF THE CONTROLLERS OF THE MICRO-GRID SIDE INVERTER.

unchanged in both amplitude and phase. As V_{ab} changes to pV, V_{bc} and V_{ca} change to qV in order to keep neutral point voltage, being $V = \sqrt{3}|V^{ref}|$ the phase-to-phase voltage reference. Let θ be phase-to-phase voltage supplementary angle and γ and x the angle and the magnitude of phase-to-neutral voltages V_a and V_b, as depicted in Fig. 4. The following equations can be deduced using their phasor relationships:

$$2qV\cos\theta = pV \tag{7}$$

$$qV\sin\theta = x\cos\gamma + \frac{V}{\sqrt{3}} \tag{8}$$

$$2x\sin\gamma = pV \tag{9}$$

$$2x\cos\gamma = \frac{V}{\sqrt{3}}. \tag{10}$$

Solving for θ and q as a function of p yields

$$\theta = atan(\frac{\sqrt{3}}{p}) \tag{11}$$

$$q = \frac{p}{2\cos\left(atan\left(\frac{\sqrt{3}}{p}\right)\right)}. \tag{12}$$

In Fig. 3, for a three-phase sag, the signal *type* is set to *balanced*, and all three phase voltage amplitudes are multiplied

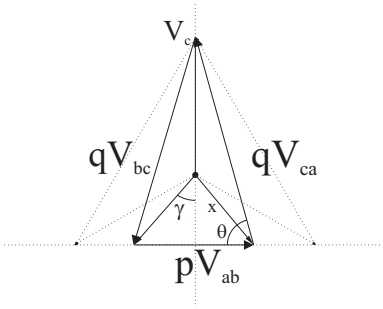

Fig. 4. Voltage phasor representation of a phase-to-phase voltage sag, type C_c.

by p during the time set as *duration*. The angles are not changed. For unbalanced sags, $type$ is set to *unbalanced* and θ and q are calculated following equations (11) and (12) respectively. Given θ and q, a three-phase voltage system is created with the following equations $V_{ab}(t) = \sqrt{2/3}pVsin(2\pi ft)$, $V_{bc}(t) = \sqrt{2/3}qVsin(2\pi ft - \pi + \theta)$ and $V_{ca}(t) = \sqrt{2/3}qVsin(2\pi ft + \pi - \theta)$.

2) Harmonic voltage generator: The harmonic voltage components are obtained from

$$v_{h\alpha} = A_h \sin\left(h\left(2\pi ft - \theta_h\right)\right) \tag{13}$$

$$v_{h\beta} = A_h \sin\left(h\left(2\pi ft - \theta_h\right) + \frac{\pi}{2}\right), \tag{14}$$

where A_h is the amplitude of the harmonic component, h is the harmonic order and $\theta_h$is the angle of the harmonic component. Therefore, by adjusting h, A_h and θ_h, the desired harmonic components are obtained, which can be added to the main voltage reference in order to obtain the distorted voltages. Equations (13) and (14) were implemented independently for 5^{th}, 7^{th} and 11^{th} harmonics so that they could be added simultaneously, as shown in Fig. 3.

3) Flicker generator: The flicker generator is a simple voltage amplitude modulation. It can either be sinusoidal or squared, with defined amplitude A_f and frequency f_f. In the present case, amplitude variation is limited to 10% and frequency to 20 Hz. These values were estimated from the P_{st} curves taken from [31], [32], which are used as means for quantifying the borderline of irritation for flicker. The application of the P_{st} value of flicker is known to be complex, and these estimations were made to clarify this function of the grid simulator.

As shown in Fig. 3, it is implemented by multiplying the voltage amplitude reference $|V^{ref}|$ by the modulation signal, a squared or sinusoidal wave with unity average value, oscillating between 1.1 and 0.9 at the desired frequency.

III. Hardware description

The topology of the test bench with the grid simulator was shown in Fig. 1. All inverters are Danfoss VLT FC302, 2.2 kW three-phase IGBT inverters. DC link has two series 385 V 2200 μF RIFA capacitors. Output filters for both inverters are LC+L, with values $L_i = L_o = 1.8mH$ and $C_f = 27\mu F$ (delta connected $3\times9\mu F$ Electronicon capacitors). The control was programmed in MATLAB/Simulink and was carried out in real-time by a ds1103 at 10 kHz. Voltage probes are 1500 V LEM LV 25-P. For currents, 50 A LEM LA 55-P probes were used. The whole set-up is shown in Fig. 5. On the left side is the grid simulator and on the right side the micro grid, with the inverter interfaced distributed

generators and the critical load. Filters and measurement boxes are also indicated in the picture. In all experiments presented in next section, V_{DC} is always 650 V.

IV. Experimental tests

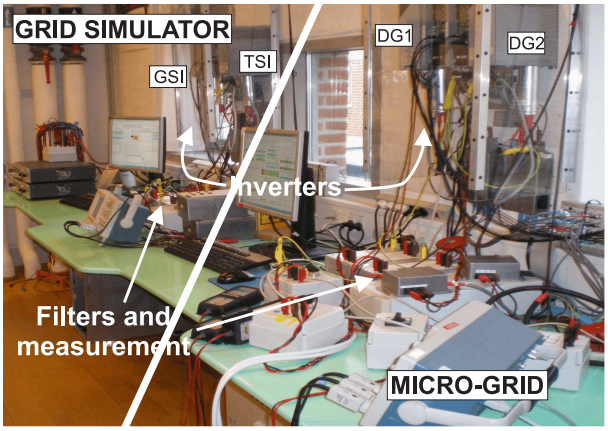

Fig. 5. The grid simulator.

The grid simulator was used to test the afore mentioned voltage disturbances on several loads: *i*) a linear purely resistive load (R=230 Ω); *ii*) a linear inductive-resistive load (R=230 Ω, L=5 mH); *iii*) a non-linear load (diode rectifier with LC filter + R=230 Ω) and *iv*) a grid-connected current-controlled inverter.

As the simulator can handle 100% bi-directional power flow, i.e. it can work in four quadrants, inverters can be operated as generator interfaces like PV or wind turbine inverters, making the grid simulator suitable for testing systems with loads and generators, such as a MG. The following results show the performance of the grid simulator under different load conditions. Some examples in each case are given, as the objective is the performance of the grid simulator, and not the behavior of the loads under such distorted voltages. In sub-section V, a case study is presented in which the behavior of a two-inverter based micro-grid is analyzed.

A. Harmonic distortion

A 200 V 50 Hz three-phase system was set in the grid simulator. A 10% of 5^{th}, 7^{th} and 11^{th} harmonic voltages were added simultaneously, as shown in Fig. 6.

Fig. 6(a) shows the currents in the resistive load R when 20 V 5^{th}, 7^{th} and 11^{th} harmonics were added to the three-phase system, shown in Fig. 6(b). The grid simulator was able to handle such distorted currents without affecting its voltages, that keep the level of harmonic distortion desired.

The response of a current controlled PV inverter, shown in Fig. 7, connected to the grid simulator with a 20 V 5^{th} harmonic is shown in Fig. 8. Figs. 8(a) and 8(b) show current and voltage respectively. Inverter current is highly distorted due to the harmonic distortion in the voltages. Nevertheless, when harmonic compensation is activated in the inverter, currents are free of harmonics despite the voltages, proving the good performance of the compensation algorithm of the tested grid-connected current-controlled inverter (Fig. 8(c)). This test clearly shows one of the applications of the

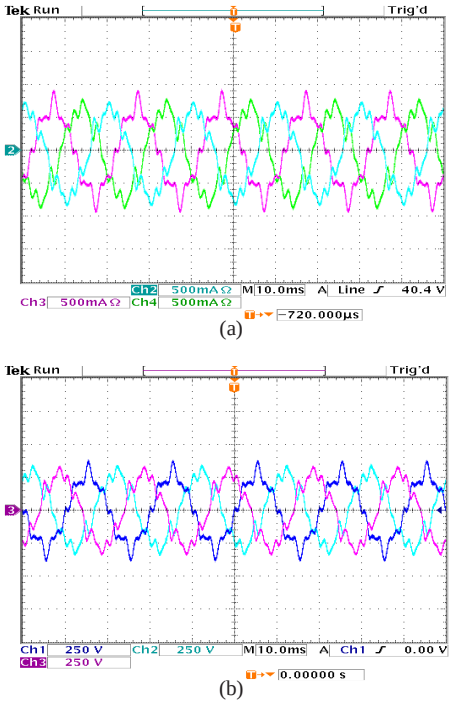

Fig. 6. Current and voltage in a resistive load when 10% 5^{th}, 7^{th} and 11^{th} harmonic are included: (a) Current and (b) Voltage.

grid simulator, such as to test power quality issues in a grid-connected inverter. This application of the grid simulator will be reinforced below in the case study of section V.

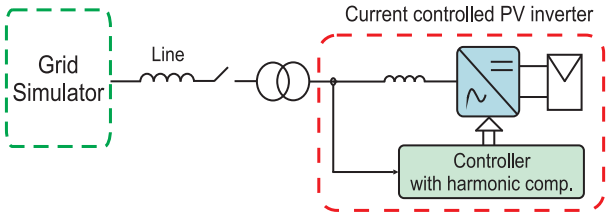

Fig. 7. Current controlled PV inverter with harmonic current compensation connected to the grid simulator.

B. Unbalanced voltages

The grid simulator is also able to generate unbalanced voltages, according to the types described in [30]. Figs. 9(a) and 9(b) show currents and voltages in the non-linear load. It is a type C unbalance with a 20% remaining voltage in phase-to-phase voltage V_{ab}. As a consequence of the reduced voltage in V_{ab}, only two braches of the rectifier are working, while the current in phase A is always zero.

Similarly, results for an inverter under unbalanced voltages are shown in Figs. 9(c) and 9(d). Again, it is a type C imbalance. The remaining voltage is now 70%. In this case, the current controlled inverter does not have separate positive and negative sequence current controllers, causing highly distorted currents. In all of the cases, the grid simulator is able to cope with the distorted currents without affecting its generated voltage waveforms.

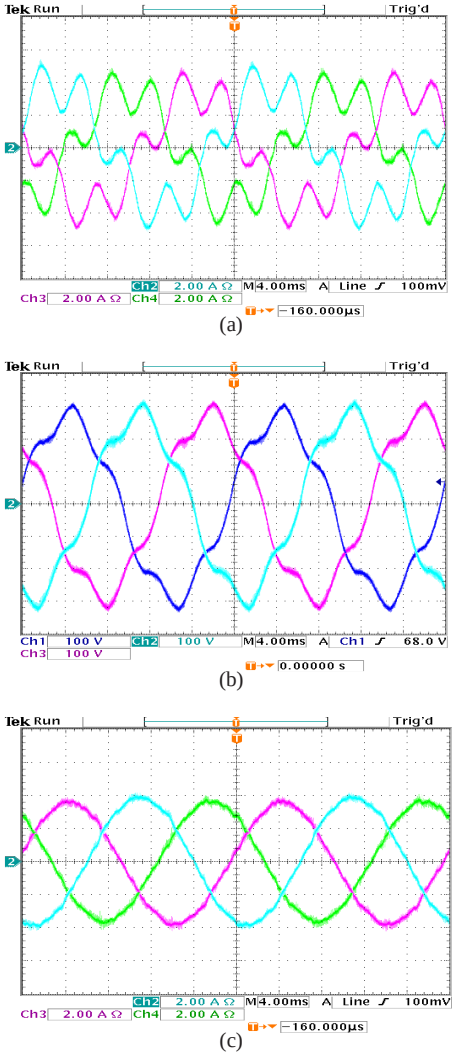

Fig. 8. Current and voltage in an inverter when 10% 5^{th} harmonic is included: (a) Current, (b) Voltage and (c) Compensated current.

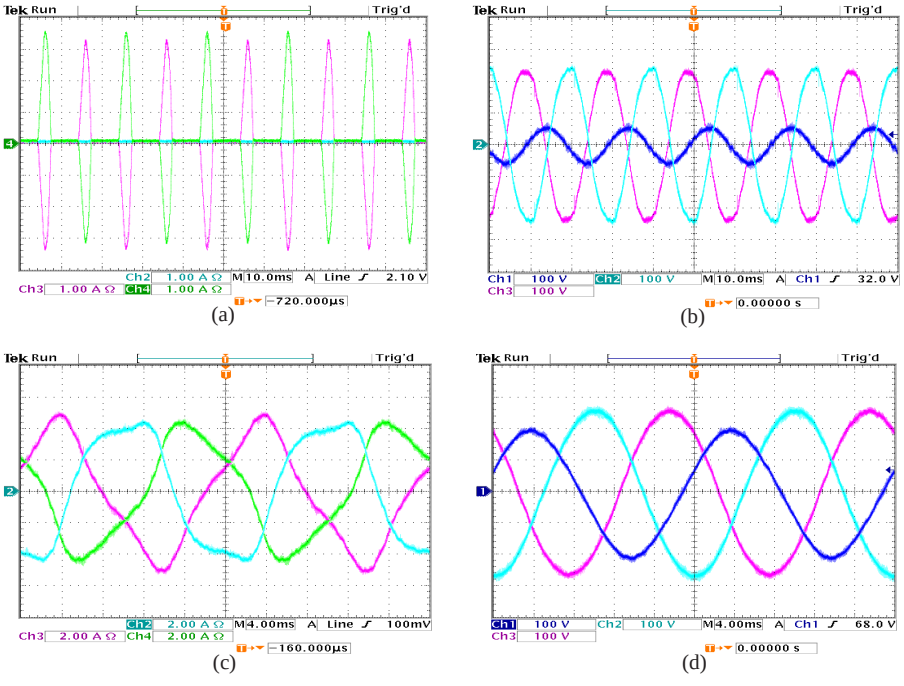

Fig. 9. Scope snapshots for unbalanced voltage tests: (a) current in a non-linear load; (b) voltage in a non-linear load; (c) current in an inverter; and, (d) voltage in an inverter

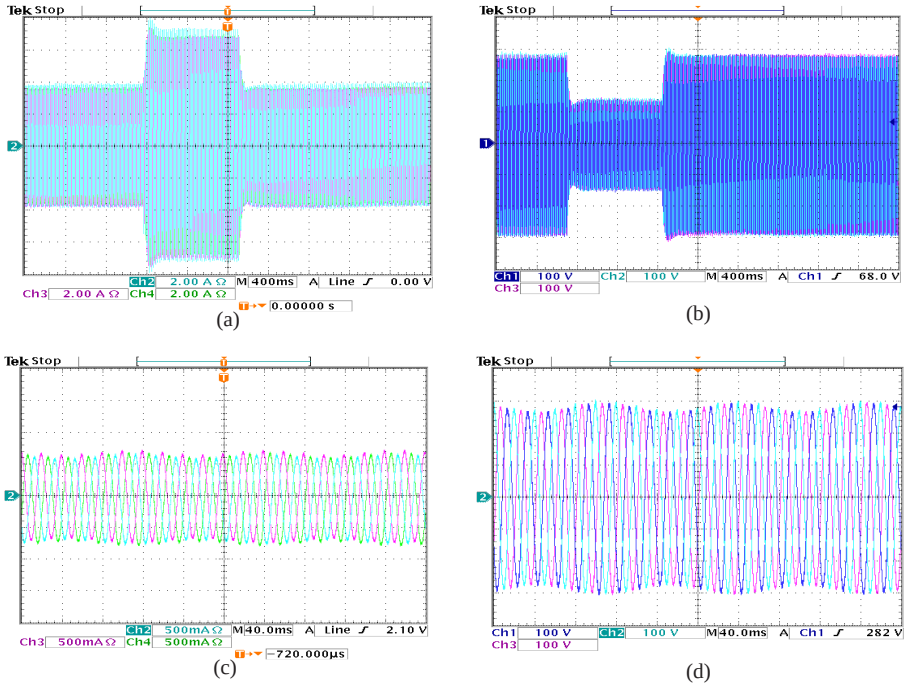

Fig. 10. Scope snapshots for voltage sags and flicker tests: (a) current in an inverter under a voltage sag; (b) voltage in an inverter under a voltage sag; (c) current in a RL load under flicker; and, (d) voltage in a RL load under flicker

C. *Voltage sags*

Figs. 10(a) and 10(b) show the response of a current controlled inverter under a three-phase voltage sag. The sag depth is 20% and its duration 550 ms, as defined by the German BDEW grid code [21]. This grid code was used as an example, but the grid simulator is able to generate different sag profiles from different grid codes, which, as discussed in the introduction, makes the grid simulator a very flexible and useful test bed. Although a voltage sag is a very abrupt change, the grid simulator showed a very good performance.

D. *Flicker*

The grid simulator can also generate low frequency oscillations in voltage amplitude, causing flicker. The response of an RL load, $R = 230\Omega$, $L = 5mH$, to flicker is shown in Figs. 10(c) and 10(d). In this case, it is a sinusoidal flicker with an amplitude of 5% of the voltage amplitude and a frequency is 8 Hz. A slight imbalance can be noticed in Fig. 10(c), which is caused by slight differences in the three-phase RL load and not by the voltages generated by the grid simulator, which do not show imbalance at all (Fig. 10(d)).

E. *Multiple disturbances*

Finally, in this section, results of combined disturbances are shown. A combination of harmonics and unbalance is shown in Fig. 11. In this case, 20 V of an 11^{th} harmonic component is added to an unbalanced voltage, being 20% the remaining voltage of phase-to-phase voltage V_{ab}. This voltage is applied to a non-linear load. Once more, the voltage reference was tracked despite the currents drawn by the load.

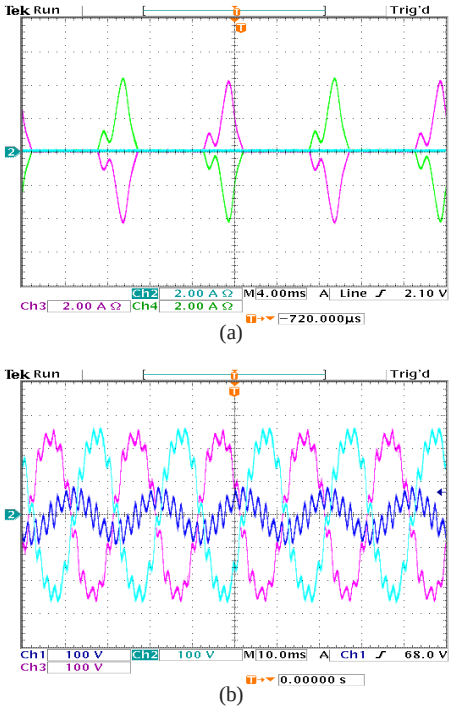

Fig. 11. Current and voltage in a non-linear load under harmonic and unblanced voltages: (a) Current and (b) Voltage

V. A CASE STUDY: COOPERATIVE UNBALANCED VOLTAGE COMPENSATION IN A MICRO-GRID

The grid simulator was also used to test a micro-grid with two inverters and a three-phase resistive load, as shown in Fig. 12. The inverters can be taken as distributed generators, while the load is considered to be the critical load in the micro-grid. All the components correspond to those presented in section III. In this case study, the grid simulator is used to generate a permanent imbalance at the point of common coupling of the micro-grid. The main idea is to maintain the quality of the voltage in the critical load, thus providing the micro-grid with a self-healing capability, being able to increase the quality of the voltage for the critical load and at the same time stay connected to the main grid, maximizing energy production even under distorted voltages.

In order to achieve this objective, the inverters of the distributed generators include unbalanced voltage compensation algorithms. Each of the distributed generators use part of their available current to compensate for the imbalance. Depending on the tuning of the imbalance compensation algorithm for each distributed generator a steady state is reached, where they share the total amount of compensation. For different generated powers, this can yield a situation in which one of the DGs is overloaded and the others still have capacity left to either generate or compensate. In this case, it is useful to limit the amount of compensation in different DGs following a certain optimization criterion mainly depending on the costs associated with the compensation.

The unbalanced voltage compensation algorithm is shown in Fig. 13. It is based on an algorithm presented in [33] for islanded micro-grids. The compensation takes into account the measured negative sequence voltage $\bar{v}^{-}_{\alpha\beta}$ and negative sequence reactive power Q^{-}. In that work, the compensation gain C was fixed in order to share the amount of Q^{-} accordingly. Here, a modification for limiting its action was included. This limitation allows us to control the amount of compensation provided by each distributed unit in the micro-grid.

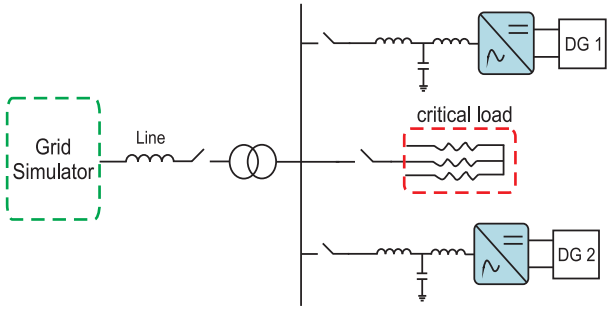

Fig. 12. Topology of the micro-grid connected to the grid simulator in the case study.

This way, different aspects in the micro-grid status can be considered for compensation purposes, such as costs of production loss, start-up time and so on. For example, if the wind is blowing, then MPPT for the wind energy distributed generator seems the best solution, but if compensation in the critical load is mandatory, then a decision must be taken, like decreasing the generated wind energy and using part of the current for compensation, or keeping MPPT for wind energy and decreasing PV generation (if any) or any other options, as many as different resources in the micro-grid.

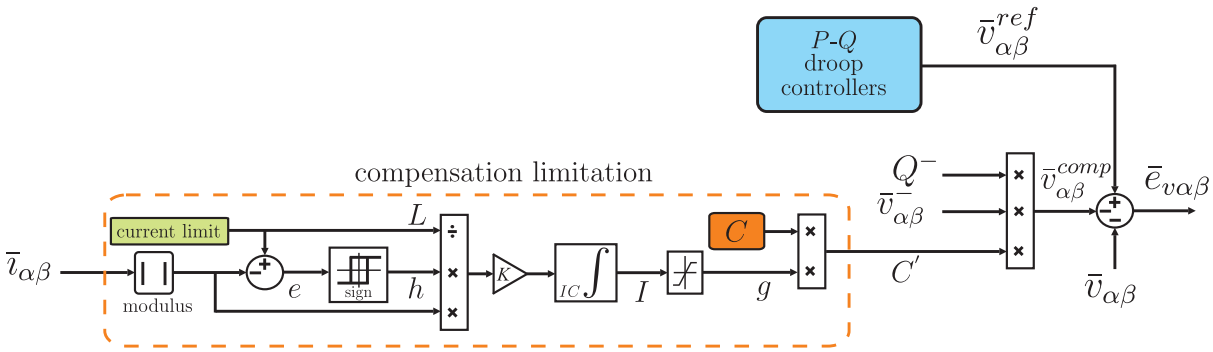

Fig. 13. Block diagram of the unbalance compensation algorithm with current limitation.

In unbalanced voltage compensation, in grid-connected case, the compensation gain C is dynamically changed as a function of the limitation of output current $\bar{i}_{\alpha\beta}$, to obtain

$$C^{'} = C \times g, \tag{15}$$

where

$$g = \begin{cases} C_u & \text{for I} > L_{upper} \\ I & \text{for I} \in [L_{lower}, L_{upper}] \\ C_l & \text{for I} < L_{lower}, \end{cases} \tag{16}$$

is the saturation function for the compensation gain, with C_u and C_l being the upper and lower limits of the saturation, L_{upper} and L_{lower} the limits of the integral and

$$I = K \int \frac{h \times |\bar{\imath}_{\alpha\beta}|}{L} dt, \tag{17}$$

is the integral of the error in the current limitation, where K is the integral gain, L is the current limit and

$$h = \begin{cases} 1 & \text{for e} > \varepsilon \\ 0 & \text{for e} \in [-\varepsilon, \varepsilon] \\ -1 & \text{for e} < -\varepsilon, \end{cases} \tag{18}$$

is a hysteresis comparator which outputs the sign of the error with a small dead band to filter out the ripple. In (18), $e = L - |\bar{\imath}_{\alpha\beta}|$ and ε is the dead band for the current limit error. The variation of the modified gain $C^{'}$ is limited to avoid excessive transient over- or under-compensation. The dead band ε used in the limitation error acts as a filter for the ripple in current modulus. The resulting compensating voltage $\bar{v}_{\alpha\beta}^{comp}$ is then subtracted from the voltage reference $\bar{v}_{\alpha\beta}^{ref}$ coming from the droop controllers. This new reference is controlled by inner voltage and current control loops.

In the present case, DG1 is generating 350 W and DG2 60 W. Unbalanced three-phase voltages are set by the grid simulator, with a 91% remainig voltage in the faulty lines. At instant t=0 s, compensation is activated for DG2. The imbalance is consequently reduced, as shown in Fig. 14(a). At around t=2.1 s, compensation is also activated for DG1. The imbalanced is further reduced until, at t=4.5 s, a current limitation of 3 A is set in DG1. The compensation effect is now limited and the unbalance factor increases again to an intermediate level.

Fig. 14(b) shows DG1 d and q current components for positive and negative sequence currents. Apart from the transients, positive sequence components do not change their values. Negative sequence component appear uncontrolled until the compensation is activated. When the current limitation is activated, current modulus stays at 3 A, as required.

The same analysis can be done by observing Fig. 14(c), where RMS values of α components of compensating voltage v_{α}^{comp}, positive sequence current i_{α}^{+} and negative sequence current i_{α}^{-} are plotted together with phase R output current i_{oR} for both distributed generators, DG1 and DG2. Positive sequence currents are only transiently affected, when either the compensation or the limitation are activated. When DG1 starts compensating, the amount of compensation in DG2 decreases, and when the limitation is activated for DG1, it increases again. A different dynamic response can also be observed as a consequence of purposely setting different compensating gain values.

Finally, the compensation effect can also be observed in Fig. 15, where the voltage at the critical load is shown before compensation (Fig. 15(a)) and after compensation (Fig. 15(b)).

This way, distributed generators in a micro-grid can act as self-healing agents, increasing voltage quality in the point of common connection and thus avoiding potential problems to critical loads. This self-healing action is done at the expense of reducing the production and dedicating part of the available current for compensation purposes, instead of generation.

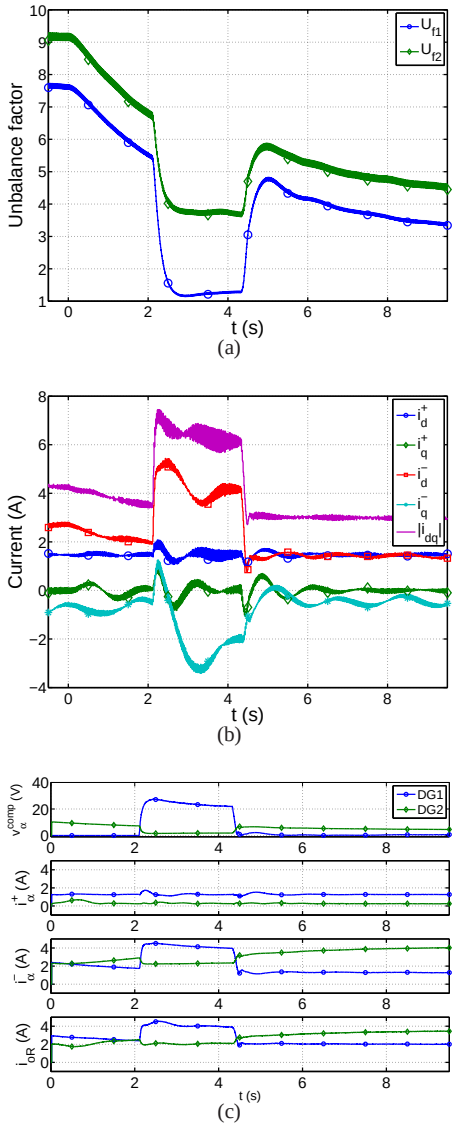

Fig. 14. Results of the case study: (a) unbalance factors for both distributed generators, (b) positive and negative sequence currents and current modulus for distributed generator 1 in dq axis, and (c) RMS values of compensating voltage, α-component positive sequence current, α-component negative sequence current and phase R output current for both distributed generators.

VI. Conclusions

In this paper, a grid simulator was designed and built. It is based on two inverters connected back-to-back, both with resonant controllers for currents and voltages. The performance of the grid simulator was tested on different kinds of loads, including linear and non-linear loads and inverters. The grid simulator had a very good performance, being able to track its reference even in the presence of very distorted currents. In addition, a case study was also presented, in which cooperative unbalanced voltage compensation was investigated in a micro-grid with two distributed generators and a critical load. The grid simulator allowed to test the compensation algorithm of the DG units in the micro-grid, proving the self-healing capability of this micro-grid as an example of possible compensation algorithm. Therefore, the grid simulator was successfully used to test power quality issues of multi-component systems such as micro-grids, where issues like Low Voltage Ride Through are likely to be mandatory in the near future, as happened with wind or PV energies, or unbalanced voltage compensation, requiring an unbalance factor of less than 3%, according to [27].

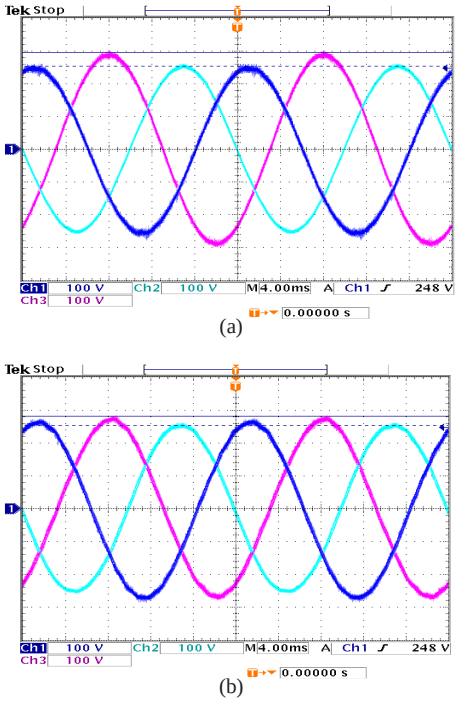

Fig. 15. Voltages at the critical load: (a) Before compensation and (b) After compensation

ACKNOWLEDGMENT

This work was partially supported by the Mobility Program of the Carlos III University Own Research Program for 2010-2011 and the Department of Energy Technology of Aalborg University.

REFERENCES

[1] A. Kahrobaeian and Y.-R. Mohamed, "Interactive distributed generation interface for flexible micro-grid operation in smart distribution systems," *Sustainable Energy, IEEE Transactions on*, vol. 3, no. 2, pp. 295 –305, april 2012.

[2] A. Basu, A. Bhattacharya, S. Chowdhury, and S. Chowdhury, "Planned scheduling for economic power sharing in a chp-based micro-grid," *Power Systems, IEEE Transactions on*, vol. 27, no. 1, pp. 30 –38, feb. 2012.

[3] D. Tran, H. Zhou, and A. Khambadkone, "Energy management and dynamic control in composite energy storage system for micro-grid applications," in *IECON 2010 - 36th Annual Conference on IEEE Industrial Electronics Society*, nov. 2010, pp. 1818 –1824.

[4] P. Lee, L. Lai, and S. Chan, "A practical approach of energy efficiency management reporting systems in micro-grid," in *Power and Energy Society General Meeting, 2011 IEEE*, july 2011, pp. 1 –5.

[5] S. Bertolini, M. Giacomini, S. Grillo, S. Massucco, and F. Silvestro, "Coordinated micro-generation and load management for energy saving policies," in *Innovative Smart Grid Technologies Conference Europe (ISGT Europe), 2010 IEEE PES*, oct. 2010, pp. 1 –7.

[6] P. M. Costa and M. A. Matos, "Economic analysis of microgrids including reliability aspects," in *Probabilistic Methods Applied to Power Systems, 2006. PMAPS 2006. International Conference on*, june 2006, pp. 1 –8.

[7] C. Wu, F. Wen, and Y. Lou, "The existed problems and possible solutions of micro-grid based on distributed generation," in *Electric Utility Deregulation and Restructuring and Power Technologies, 2008. DRPT 2008. Third International Conference on*, april 2008, pp. 2763 –2768.

[8] R. Cuzner and G. Venkataramanan, "The status of dc micro-grid protection," in *Industry Applications Society Annual Meeting, 2008. IAS '08. IEEE*, oct. 2008, pp. 1 –8.

[9] S. Dasgupta, S. Mohan, S. Sahoo, and S. Panda, "A plug and play operational approach for implementation of an autonomous-micro-grid system," *Industrial Informatics, IEEE Transactions on*, vol. PP, no. 99, p. 1, 2012.

[10] D. Vilathgamuwa, P. C. Loh, and Y. Li, "Protection of microgrids during utility voltage sags," *Industrial Electronics, IEEE Transactions on*, vol. 53, no. 5, pp. 1427 –1436, oct. 2006.

[11] P. Tenti, A. Costabeber, and P. Mattavelli, “Improving power quality and distribution efficiency in micro-grids by cooperative control of switching power interfaces,” in *Power Electronics Conference (IPEC), 2010 International*, june 2010, pp. 472 –479.

[12] J. Cobben, W. Kling, and J. Myrzik, “Power quality aspects of a future micro grid,” in *Future Power Systems, 2005 International Conference on*, nov. 2005, pp. 5 pp. –5.

[13] Y. Chung, G. Kwon, T. Park, H. Kim, and J. Moon, “Voltage sag, swell and flicker generator with series injected inverter,” in *Power Engineering Society General Meeting, 2005. IEEE*, june 2005, pp. 1308 – 1313 Vol. 2.

[14] R. Lohde and F. Fuchs, “Laboratory type pwm grid emulator for generating disturbed voltages for testing grid connected devices,” in *Power Electronics and Applications, 2009. EPE ’09. 13th European Conference on*, sept. 2009, pp. 1 –9.

[15] R. Zhang, M. Cardinal, P. Szczesny, and M. Dame, “A grid simulator with control of single-phase power converters in d-q rotating frame,” in *Power Electronics Specialists Conference, 2002. pesc 02. 2002 IEEE 33rd Annual*, vol. 3, 2002, pp. 1431 – 1436 vol.3.

[16] R. Majumder, A. Ghosh, G. Ledwich, and F. Zare, “Power management and power flow control with back-to-back converters in a utility connected microgrid,” *Power Systems, IEEE Transactions on*, vol. 25, no. 2, pp. 821 –834, may 2010.

[17] ——, “Load sharing and power quality enhanced operation of a distributed microgrid,” *Renewable Power Generation, IET*, vol. 3, no. 2, pp. 109 –119, june 2009.

[18] R. Ray, D. Chatterjee, and S. Goswami, “Reduction of voltage harmonics using optimisation-based combined approach,” *Power Electronics, IET*, vol. 3, no. 3, pp. 334 –344, may 2010.

[19] T. Bhattacharya and L. Umanand, “Negative sequence compensation within fundamental positive sequence reference frame for a stiff micro-grid generation in a wind power system using slip ring induction machine,” *Electric Power Applications, IET*, vol. 3, no. 6, pp. 520 –530, november 2009.

[20] BOE, “P.O. 12.2. Draft: Installations connected to the transport system: design, equipment, performance and security,” *BOE*, 2010.

[21] BDEW, *Technical Guideline: Generating plants connected to the medium-voltage network.* Berlin, Germany: BDEW Bundesverband der Energie- und Wasserwirtschaft e.V., June 2008.

[22] (2012, April) Regolazione tecnica dei requisiti di sistema della generazione distribuita Allegato A.70 Codice di Terna. http://www.allegatoa70.it/?p=22. Last accessed on 12 august 2012.

[23] (2012, Feb) NERC Standar PRC-024-1: Generator Performance During Frequency and Voltage Excursions. http://www.nerc.com/filez/standards/Generator-Verification-Project-2007-09.html. Last accessed on 19 july 2012.

[24] (2012, June) The grid code, issue 4, rev 13. http://www.nationalgrid.com/uk/Electricity/Codes/gridcode/updates/. Last accessed on 19 july 2012.

[25] JORF, *Arrêté du 23 avril 2008 relatif aux prescriptions techniques de conception et de fonctionnement pour le raccordement á un réseau public de distribution d’électricité en basse tension ou en moyenne tension d’une installation de production d’énergie électrique.* Paris, France: Journal officiel de la République française, April 2008.

[26] (2005) National Guidance Catalogue for Renewable Energy Industry Development (NDRC Energy [2005] No. 2517). http://www.cwpc.cn/cwpc/en/node/6548. Last accessed on 19 july 2012.

[27] “Ieee guide for design, operation, and integration of distributed resource island systems with electric power systems,” *IEEE Std 1547.4-2011*, pp. 1–54, 2011.

[28] D. Zmood and D. Holmes, “Stationary frame current regulation of pwm inverters with zero steady-state error,” *Power Electronics, IEEE Transactions on*, vol. 18, no. 3, pp. 814 – 822, may 2003.

[29] M. Castilla, J. Miret, J. Matas, L. Garcia de Vicuna, and J. Guerrero, “Control design guidelines for single-phase grid-connected photovoltaic inverters with damped resonant harmonic compensators,” *Industrial Electronics, IEEE Transactions on*, vol. 56, no. 11, pp. 4492 –4501, nov. 2009.

[30] M. Bollen, “Algorithms for characterizing measured three-phase unbalanced voltage dips,” *Power Delivery, IEEE Transactions on*, vol. 18, no. 3, pp. 937 – 944, july 2003.

[31] IEEE-1453-2004, *Measurement and Limits of Voltage Fluctuations and Associated Light Flicker on AC Power Systems.* IEEE, 2004.

[32] IEC-61000-3-7, *Technical report. Electromagnetic compatibility (EMC). Part 3-7: Limits - assessment of emission limits of the connection of fluctuating installations to MV, HV and EHV.* International Electrotechnical Commission, 2008.

[33] M. Savaghebi, J. Guerrero, A. Jalilian, and J. Vasquez, “Experimental evaluation of voltage unbalance compensation in an islanded microgrid,” in *Industrial Electronics (ISIE), 2011 IEEE International Symposium on*, june 2011, pp. 1453 –1458.